Heliyon 10 (2024) e38300

Contents lists available at ScienceDirect

Heliyon

journal homepage: www.cell.com/heliyon

Research article

Synthesis, characterization, quantum mechanical calculations and biomedical docking studies on curcumin analogs: 2, 6-(Difurfurylidene) cyclohexanone and 2, 6 – Bis (2,6-Dichloro Benzylidene) Cyclohexanone

S. Sathiyamoorthi [a], Meganathan Chandrasekaran [a,*], K. Thiruppathi [b], P. Padmanathan [c], S. Subashchandrabose [d,**], S. Gomathi [e]

[a] Department of Physics, Sri Sai Ram Engineering College, Tambaram, Chennai, 600 044, Tamil Nadu, India
[b] Department of Physics, SRM Valliammai Engineering College, SRM Nagar, Kattankulathur, Kanchipuram, 603203, India
[c] School of Mechanical Engineering, Vellore Institute of Technology, Vellore, 632014, India
[d] Centre for Functionalized Materials, Department of Physics, PRIST Deemed University, Thanjavur, 613403, Tamilnadu, India
[e] Department of Chemistry, Periyar Maniammai Institute of Science and Technology, Thanjavur, 613403, Tamilnadu, India

ARTICLE INFO

Keywords:
Colorectal cancer
Density functional theory
Molecular docking
HOMO-LUMO
Curcumin

ABSTRACT

The initiation of colorectal cancer is controlled by various factors, including random occurrences and genetic alterations affecting oncogenes and tumor suppressor genes.Curcumin, a significant compound extracted from turmeric, has attracted interest for its robust anticancer properties, particularly regarding its analogs, 2, 6-bisdifurfurylidene cyclohexanone (DFC) and 2, 6-bis (2, 6-dichlorobenzylidene) cyclohexanone (DCC), which were synthesized and assessed for their anticancer efficacy. A combination of spectroscopic techniques and molecular docking methods was utilized to comprehensively evaluate the interaction behaviors of DFC and DCC. The application of density functional theory (DFT) using the B3LYP/6-311G (d, p) basis set facilitated the prediction of spectroscopic properties. The molecular docking investigations conducted using the Glide docking program from Schrodinger Maestro elucidated the interactions of these drugs at the molecular level. In vitro investigations were performed to evaluate the cytotoxic efficacy of the synthesized curcumin analogs. The determined IC_{50} values revealed that DFC displayed an IC_{50} of approximately 82 μM, and DCC exhibited a significantly lower IC_{50} of around 10 μM. This notable disparity highlights the potential of DFC and DCC as a more efficacious cytotoxic agent and further research be conducted on the produced chemicals in the future.

1. Introduction

The design and synthesis of novel integrated synthetic organic compounds that incorporate two or more potentially bioactive substructures of small molecules for drug discovery [1]. Specifically, heterocyclic compounds containing furan, pyran, pyrrole, thiophene, and thiazole moieties exhibit ant parasitic, antibacterial, anxiolytic, ant arrhythmic, antifungal, and anticancer properties

* Corresponding author.
** Corresponding author.
E-mail addresses: megac2005@gmail.com (M. Chandrasekaran), sscbphysics@gmail.com (S. Subashchandrabose).

https://doi.org/10.1016/j.heliyon.2024.e38300
Received 16 July 2024; Received in revised form 20 September 2024; Accepted 20 September 2024
Available online 27 September 2024

[2–7]. Moreover, antimicrobial inhibitors with functional substitution organic molecules play a critical role compared to non-substituted compounds [8]. Organic small compounds that are facile to synthesize, exhibit bioavailability, and show potential antibacterial activities that are not influenced by bacterial resistance [9]. Additionally, a distinctive mechanism of action to address medication resistance has been examined.

Due to its extensive biological actions, curcumin serves as a traditional medicine in numerous Asian nations. Notwithstanding, it possesses disadvantages including inadequate absorption, restricted tissue distribution, and fast metabolism [10]. Therefore, the alteration of specific functional groups in curcumin that enhance its bioavailability will augment its efficacy. Numerous strategies exist to augment the bioavailability of curcumin, including liposomal formulation, nanoparticle manufacturing, and the synthesis of synthetic molecules to block metabolic enzymes [11–15]. In the current study, two compounds were synthesized: one is 2,6-bisdifurfurylidene cyclohexanone (DFC), where the β-diketone is substituted with a stable cyclohexanone structure and the phenolic ring is replaced by a furan ring; the other is 2,6-bis(2,6-dichlorobenzylidene) cyclohexanone (DCC), in which the β-diketone is substituted with a stable cyclohexanone structure and chlorine atoms are introduced at the 2,6 positions in place of hydroxy and methoxy groups [16]. Cyclohexane comprises a ring of six carbon atoms, also referred to as Hexanaphthene. The distinctive function of these molecules is to inhibit the transport of low molecular weight hydrophilic compounds into bacterial cells [17]. Experimental evidence indicates that cyclohexane derivatives are crucial for biological activities such as anticancer, antioxidant, cytotoxic, analgesic, anti-inflammatory, and antithrombin effects, and they exhibit superior solubility in aqueous solutions compared to curcumin analogs [18]. Mapoung et al., observed that cyclohexane exhibited a more potent inhibitory effect than curcumin analogs [19]. According to the study by Wei X et al., cyclohexane derivatives demonstrate enhanced efficacy in causing apoptosis and suppressing nuclear factor kappa B (NF-κB) [20]. Additionally, it possesses anti-cancer and antibacterial properties and plays a vital role in the management of diabetes mellitus and hypertension [17].

The physiochemical properties of synthetic compounds have been examined using spectroscopic methods including ^{1}H nuclear magnetic resonance (NMR), ^{13}C NMR, Fourier transform infrared (FT-IR), Fourier transform Raman (FT-Raman), and ultraviolet–visible spectroscopy (UV–Vis). Density functional theory is essential in the development of new pharmaceuticals, and quantum mechanical research methods are accurate in the pharmaceutical field [20]. Consequently, DFT calculations utilizing the B3LYP/6-311G (d, p) basis set have been employed to determine the optimal geometry, dipole moment, polarizability, E_{HOMO}-E_{LUMO} energy, and excited state energy [21]. Furthermore, a computer-aided drug design (CADD) and molecular docking studies were conducted to elucidate the binding mechanism and binding energy between the ligand and the macromolecule (protein). Furthermore, we evaluated the in-vitro cytotoxic effects of DFC and DCC on conventional cancer cell lines and established their IC_{50} values.

2. Materials and methods

2.1. Synthesis details

Aldol condensation is employed for synthesis as per the strategy delineated in Refs. [22,23]. Chemicals were employed without further purification after acquisition as LR grades. Fifty millilitres of ethanol, 0.01 mol of cyclohexanone, 0.02 mol of furfuraldehyde, and 0.02 mol of 2,6-dichlorobenzaldehyde were introduced into a beaker. Ten percent catalyst (NaOH) was introduced. Two drops of concentrated HCl were introduced to neutralize the alkali after the items were combined with ice-cold water. The crude products of 2, 6-Difurfurylidene cyclohexanone (DFC) and 2,6-Bis(2,6-dichlorobenzylidene) cyclohexanone (DCC) were subjected to multiple

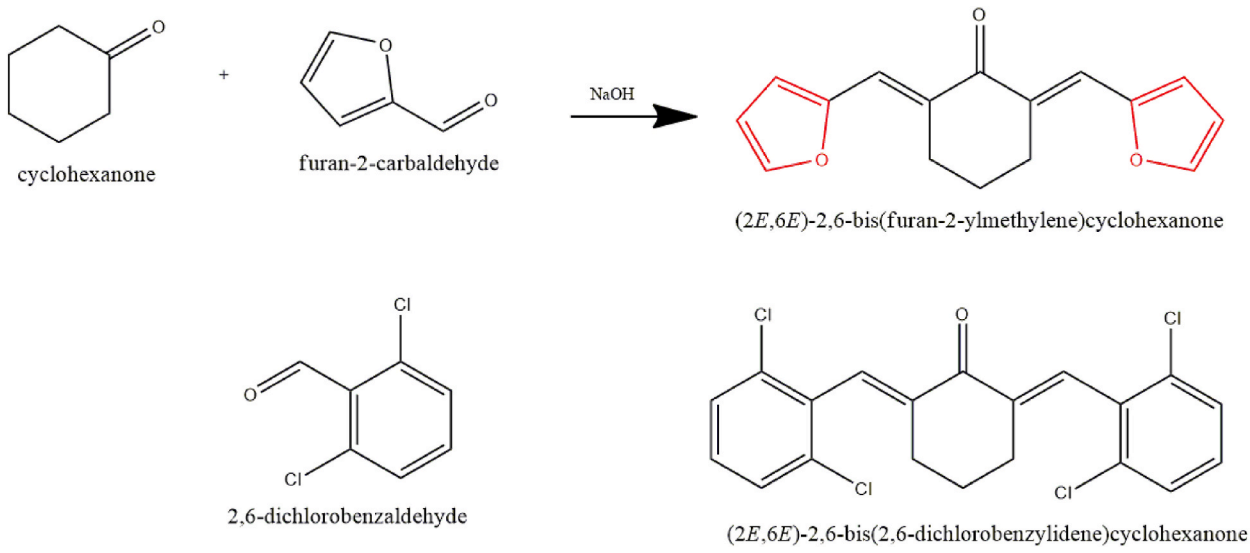

Fig. 1. Synthesis procedure of DFC and DCC.

washes with distilled water and subsequently dried. Acetone and chloroform served as solvents for the recrystallization of products DFC and DCC, respectively. Fig. 1 illustrates the reaction scheme. Cyclohexanone, furfuraldehyde, and 2,6-dichlorobenzaldehyde were acquired from Sigma Aldrich in laboratory reagent grade. They were utilized for synthesis without undergoing purification. The FT-IR spectrum was obtained using the JASCO 6300 FT-IR spectrometer, equipped with a DTGS detector and a KBr beam splitter. The spectral resolution was 1.92847 cm^{-1}, encompassing the range of 400–4000 cm^{-1}. A BRUKER RFS 27, a standalone FT-Raman spectrometer with a spectral resolution of 2 cm^{-1} and an excitation wavelength of 1064 nm from an Nd: YAG laser source was utilized to acquire the FT-Raman spectrum. A Shimadzu-UV 2600 UV–vis spectrophotometer was employed to get the crystal's UV–Vis absorption spectra within the 200–800 nm wavelength range. PAN analysis utilized XpertPRO, with a step size of 0.017 for theta and a Cu Kα wavelength of 1.54 × 10^{-10} m. PowderX software is employed to index the pattern and lattice characteristics. Density Functional Theory computations were conducted using Gaussian 09W. Powder X-ray diffraction (XRD) studies employed PAN analytical and XpertPRO to determine the lattice parameters. The Cu Kα wavelength of 1.54 Å and a step size of 0.017 for theta were employed. The pattern is indexed with PowderX [24] software, and lattice parameters are calculated for DFC and DCC. The values are subsequently compared with single crystal XRD measurements and summarized in Table 1. Indexed patterns are contrasted with simulated patterns derived from Mercury [25] and presented in Fig. 2a and b for DFC and Fig. 2c and d for DCC with XRD data [26,27]. The single crystal crystallographic data can be accessed in the Cambridge Structural Database (CSD) using the following database IDs: (i) ID: XOZWOZ, CCDC: 758293 for the DFC molecule and ID: LAPROL, CCDC: 872542 for the DCC molecule.

2.2. ^{1}H and ^{13}C NMR analysis

DFC-^{1}H NMR: CH_2: 1.9, 2.9 ppm; C=CH: 7.3 ppm; C-H: 7.5, 6.4, 6.8 ppm; DCC- ^{1}H NMR: CH_2: 1.9, 2.8 ppm; C=CH: 7.6 ppm; Chlorobenzene ring proton: 7.3, 7.1 ppm. DFC- ^{13}C NMR: C=O: 189.01 ppm; Cyclohexan ring carbon: 116.39 ppm; CH_2:21.6, 27.98 ppm; C=CH: 133.03 ppm, carbon in the Furaldehyde: 152.77, 112.52, 112.32, 144.52 ppm| DCC-^{13}C NMR: C=O: 188.09 ppm; Cyclohexan ring carbon: 140.15 ppm, CH_2: 30.94, 28.21 ppm; C=CH: 137.28 ppm; Carbon in Chlorobenzene ring: 135.64, 129.43, 134.29, 132.29 ppm.

The ^{1}H and ^{13}C NMR spectra were obtained for both DFC and DCC, and calculations were performed using the HF/6-31G (d, p) basis set. The observed and estimated results align well with one another. The aromatic protons were detected in the range of 6.4–7.5 ppm. The methylidene proton exhibited chemical shifts of 7.3 and 7.6 ppm in both compounds, with corresponding calculated values of approximately 9.71 and 8.96 ppm, respectively [28]. The methylene protons of cyclohexanone were detected at higher fields of 1.9 and 2.9 ppm in DFC and 1.9 and 2.8 ppm in DCC. Furthermore, protons in Furaldehyde are detected at 6.4, 6.8, and 7.5 ppm (HF: 7.44, 7.19, 8.45 ppm), while in Chlorobenzene, they are identified at 7.3 and 7.1 ppm (HF: 8.12, 8.14, 8.07 ppm).

In the ^{13}C NMR spectra of chalcones, the carbonyl carbon typically resonates between δ186.6 and δ196.8 [29–34]. In 2,6-Bis-furan-2-ylmethylene-cyclohexanone, the carbonyl carbon typically resonates at 189 ppm in DFC and 188.09 ppm in DCC. The α- and β-carbon atoms relative to the carbonyl group exhibit distinctive signals ranging from δ116.39 to δ133.03 in DFC and from δ140.15 to δ137.28 in DCC [34–36]. Furthermore, the carbon atoms in the Furaldehyde ring are observed at 152.77, 112.52, 112.32, and 144.52 ppm, whereas the carbon atoms in the Chlorobenzene ring are noted at 135.64, 129.43, 134.29, 132.29, and 135.64 ppm. The computed values for the aforementioned categories align well with the experimental data. Furthermore, both data corroborate the functional groups identified in the chemical structures of DFC and DCC. The results acquired from both experimental and computational methods are presented in Tables 2 and 3. The NMR spectra are presented in Figs. S1–S4 (Supporting Information).

2.3. Puckering analysis

The extent of the ring puckering [37] can be obtained from the puckering amplitude (Q) and the value for DFC and DCC are found to be 0.506(3)Å and 0.534 (3) Å respectively indicate that both the molecule have a significant deviation from planarity. The six membered ring (C1-C2-C3-C4-C3-C2) of DCC and DFC adopt a twist boat conformation which is evident from the θ values of 59.7(4)° and 64.4 (3) ° respectively. This twisted boat conformation arises due to the steric effects, which are present in both of the molecule. The phase angle (φ) provide the orientation of the puckering in three dimensional space and the value for DFC and DCC are found to be 180.0 (3)°& 180.0 (4)° respectively which indicate that there is a symmetrical puckering that occurs within the ring.

Table 1
Lattice parameter of the DFC and DCC.

Lattice parameter system	DFC		DCC	
	Literature value [18]	Calculated by Powder XRD	Literature value [19]	Calculated by Powder XRD
	Orthorhombic *Pnma*	Orthorhombic *Pnma*	Orthorhombic *Pna*2_1	Orthorhombic *Pna*2_1
a	7.7313 (11) Å	7.753	17.917 (4)	17.917
b	15.658 (2) Å	15.637	7.3094 (15)	7.309
c	10.3388 (14) Å	10.401	14.093 (3)	14.079
Volume	1251	1260	1845	1845

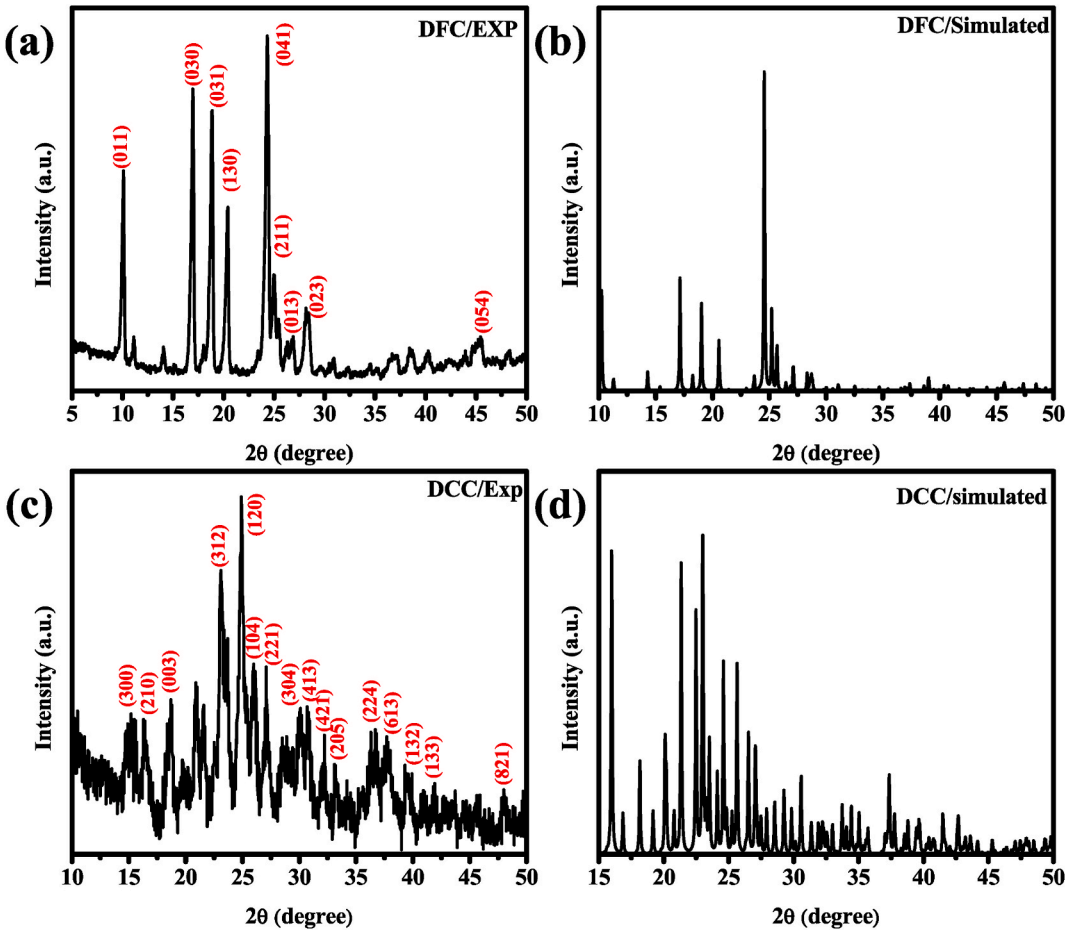

Fig. 2. XRD and simulated pattern of DFC (a & b) and DCC (c & d).

Table 2
The experimental (^{1}H) and computed (HF/6-31G(d,p)) NMR results of DFC and DCC molecules.

S.No	DFC			DCC		
	Functional groups	^{1}H NMR (ppm)	HF/6-31G(d,p)	Functional groups	^{1}H NMR (ppm)	HF/6-31G(d,p)
1	Methylene proton	1.9, 2.9	2.28, 2.06 3.18, 2.86 2.86, 3.18	Methylene proton	1.9, 2.8	1.92, 1.75 2.96, 2.51 2.51, 2.96
2	Methyledine proton	7.3	9.17, 9.17	Methyledine proton	7.6	8.96, 8.96
3	Furaldehyde proton	7.5, 6.4, 6.8	7.44, 7.19, 8.45	Chlorobenzene ring proton	7.3, 7.1	8.12, 8.14, 8.07 8.12, 8.14, 8.07

2.4. Molecular docking

The binding efficiency of compounds was analyzed using Glide docking algorithm provided by Schrodinger maestro packages. The protein of colon cancer [38] (PDB ID: 1DI8) directly downloaded from RCSB database and prepared using protein prep wizard. It includes elimination of water molecules, insertion of lost hydrogen atom and clean up the protein structure [39]. Consequently, ligprep module was used to prepare the ligand molecules for docking [39,40]. Glide docking examine protein and ligand molecules based on the two criteria (i) grid based energetic ligand docking (ii) desirable interaction. Therefore, the grid in the active region of the macro structure was formed using the receptor grid production wizard. Three modules, (i) High throughout virtual screening (HTVS), (ii) standard precision (SP) docking, and (iii) extra precision (XP) docking, procedure available in Glide. Of the 3, extra precision docking was performed for all 3 compounds. The binding affinities of the compounds were then analyzed using xp-score available in Glide.

Table 3
The experimental (^{13}C) and computed (HF/6-31G(d,p)) NMR results of DFC and DCC molecules.

S. No	DFC			DCC		
	Functional groups	^{13}C NMR (ppm)	HF/6-31G(d,p)	Functional groups	^{13}C NMR (ppm)	HF/6-31G(d,p)
1	Carbonyl carbon	189.01	186.72	Carbonyl carbon	188.09	187.20
2	Cyclohexan ring carbon	116.39	126.71, 126.71	Cyclohexan ring carbon	140.15	135.44, 135.44
3	Methylene Carbon	21.6, 27.98	19.10, 24.22, 24.22	Methylene Carbon	30.94, 28.21	19.25, 24.11, 24.11
4	Methyledine carbon	133.03	132.61, 132.61	Methyledine carbon	137.28	135.63, 135.63
5	Furaldehyde carbon	152.77, 112.52, 112.32, 144.52	150.06, 150.06 115.08, 115.08 108.45, 108.45 144.52, 144.52	Chlorobenzene ring carbon	135.64, 129.43, 129.43 134.29, 134.29, 132.29,	135.98 139.58 139.24 127.75 127.75 127.41

Table 4
The optimized geometrical bond length (Å) parameters of DFC & DCC using experimental and computational (DFT) studies.

S.No	DFC			DCC		
	Bond length	**DFT**	**Crystal** [19]	**Bond length**	**DFT**	Crystal [18]
1	C1-C2	1.510	1.507	C1-C2	1.501	1.482
2	C1-C6	1.510	1.492	C1-C6	1.500	1.482
3	C1-O25	1.218	1.228	C1-O7	1.226	1.235
4	C2-C3	1.511	1.51	C2-C3	1.511	1.506
5	C2-C16	1.340	1.337	C2-C14	1.354	1.344
6	C3-C4	1.531	1.524	C3-C4	1.530	1.510
7	C3-H26	1.099	0.97	C3-H20	1.100	0.97
8	C3-H27	1.091	0.97	C3-H21	1.089	0.97
10	C4-C5	1.533	1.523	C4-C5	1.530	1.510
11	C4-H28	1.094	0.97	C4-H22	1.094	0.97
12	C4-H29	1.095	0.97	C4-H23	1.096	0.97
13	C5-C6	1.509	1.502	C5-C6	1.510	1.506
14	C5-H30	1.098	0.97	C5-H24	1.100	0.97
15	C5-H31	1.093	0.97	C5-H25	1.095	0.97
16	C6-C7	1.343	1.331	C6-C8	1.354	1.344
17	C7-C8	1.477	1.483	C8-C9	1.433	1.426
18	C7-H32	1.087	0.93	C8-H26	1.086	0.93
19	C8-C9	1.407	1.399	C9-C10	1.379	1.355
20	C8-C13	1.406	1.396	C9-O13	1.380	1.377
21	C9-C10	1.388	1.385	C10-C11	1.423	1.410
22	C9-Cl15	1.758	1.7414	C10-H27	1.076	0.93
23	C10-C11	1.391	1.388	C11-C12	1.362	1.336
24	C10-H33	1.082	0.93	C11-H28	1.078	0.93
25	C11-C12	1.389	1.388	C12-O13	1.352	1.352
26	C11-H34	1.083	0.93	C12-H29	1.077	0.93
27	C12-C13	1.391	1.388	C14-C15	1.431	1.426
28	C12-H35	1.082	0.93	C14-H30	1.086	0.93
29	C13-Cl14	1.758	1.737	C15-C16	1.376	1.355
30	C16-C17	1.481	1.484	C15-O19	1.376	1.377
31	C16-H36	1.087	0.93	C16-C17	1.423	1.410
32	C17-C18	1.404	1.399	C16-H31	1.079	0.93
33	C17-C22	1.404	1.396	C17-C18	1.361	1.355
34	C18-C19	1.391	1.386	C17-H32	1.078	0.93
35	C18-Cl24	1.759	1.742	C18-O19	1.357	1.355
36	C19-C20	1.390	1.382	C18-H33	1.077	0.93
37	C19-H37	1.082	0.93			
38	C20-C21	1.390	1.38			
39	C20-H38	1.083	0.93			
40	C21-C22	1.389	1.391			
41	C21-H39	1.082	0.93			
42	C22-Cl23	1.758	1.743			

2.5. Cell culture

The homo-sapiens colon cancer cell line HCT116 was cultivated in a medium that contained Dulbecco's Modified Eagle Serum (1 % Penicillin, Streptomycin, and Amphotericin), 10 % Fetal Bovine Serum, and 10 % Fetal Bovine Serum. The temperature of the cells was kept at 37 °C in a humidified environment with 5 % CO_{23}.

3. Results and discussions

3.1. Molecular geometry

The molecular structure of DFC and DCC [41–44] were optimized using B3LYP/6-311G (d, p) level of basis set [45]. The optimized bond parameters of both DFC and DCC were compared and discussed the changes in geometries. The bond parameters are given in Tables 4 and 5. The optimized molecular structure of DFC and DCC is given in Figs. 3 and 4.

There is a lot of analogy in both structure due to the substitutions, in DFC the five member ring furan substituted in 2, 6 position of Cyclohexanone. The calculated bond length of carbonyl group (C=O) in DFC is 1.226 Å and 1.218 Å in DCC. It seems the C=O bond in DFC is elongated about 0.008 Å than the DCC. Whereas, the bonds C1-C2 and C1-C6 in both DFC and DCC are showing a difference approximately 0.009 Å, here exhibit contraction of bond length in DFC. Moreover, the bond linked between the 2 and 6 position is 1.354 Å (in both DFC), but in DCC the bond lengths are about 1.343 Å (C6=C7) and 1.340 Å (C2=C16) are shrinked about ~0.011 Å. These differences are due to delocalization of charges about 20.33 and 18.28 kcal/mol from electronegative furan and Chlorobenzene respectively, to Cyclohexanone ring. The charge delocalization natural bond orbitals (NBO) are listed in Table 6.

On the other hand, the bonds in Cyclohexanone ring other than linkage not shown any major difference, it clearly shows that the charge delocalization mostly locates over the link between the 2, 6 positions. The chair conformation is energetically favored for Cyclohexanone [46]. The calculated torsion angles of C2-C3-C4-C5, C3-C4-C5-C6, C4-C5-C6-C1, C2-C1-C6-C5, C6-C1-C2-C3, and C1-C2-C3-C4 are about −58.91°, 53.39°, −20.62°, −6.73°, 0.92° and 31.58°, respectively, ascertained the chair conformation. It is due to ethylene groups attached at the 3, 4 and 5 positions in Cyclohexanone and hence the lowered the dihedral angles. Due to absence of

Table 5
The optimized geometrical bond angles (°) of DFC & DCC using experimental and computational (DFT) studies.

DFC						DCC					
Angle (°)	DFT	Crystal	DFC	DFT	Crystal	Angle (°)	DFT	Crystal	DCC	DFT	Crystal
C2-C1-C6	118.18	118.2	C1-C6-C8	115.86	117.8	C2-C1-C6	117.945	117.45	C10-C9-Cl15	118.066	118.69
C2-C1-O7	121.01	120.85	C5-C6-C8	123.84	122.7	C2-C1-O25	121.025	121.32	C9-C10-C11	119.148	118.97
C6-C1-O7	120.80	120.85	C6-C8-C9	128.90	–	C6-C1-O25	120.999	121.19	C9-C10-H33	119.706	120.5
C1-C2-C3	119.13	119.5	C6-C8-H26	116.31	115.9	C1-C2-C3	119.230	119.47	C11-C10-H33	121.145	120.5
C1-C2-C14	115.49	–	C9-C8-H26	114.79	115.9	C1-C2-C16	116.232	116.69	C10-C11-C12	120.203	120.36
C3-C2-C14	125.37	–	C8-C9-C10	137.00	137.00	C3-C2-C16	124.536	123.82	C10-C11-H34	119.907	119.8
C15-C16-C17	107.13	–	C8-C9-O13	114.60	114.73	C2-C3-C4	112.118	112.35	C12-C11-H34	119.888	119.888
C15-C16-H31	125.38	–	C10-C9-O13	108.38	108.2	C2-C3-H26	108.444	109.1	C11-C12-C13	119.513	119.513
C17-C16-H31	127.48	–	C9-C10-C11	107.09	107.6	C2-C3-H27	110.317	109.1	C11-C12-H35	120.996	120.996
C16-C17-C18	106.00	–	C9-C10-H27	126.38	126.2	C4-C3-H26	108.492	109.1	C13-C12-H35	119.488	119.488
C16-C17-H32	127.61	–	C11-C10-H27	126.51	126.2	C4-C3-H27	110.923	109.1	C8-C13-C12	122.465	122.465
C18-C17-H32	126.39	–	C10-C11-C12	106.11	106.4	H26-C3-H27	106.330	107.9	C8-C13-Cl14	120.268	120.268
C17-C18-O19	110.74	–	C10-C11-H28	127.37	126.8	C3-C4-C5	110.081	109.69	C12-C13-Cl14	117.220	117.220
C17-C18-H33	133.44	–	C12-C11-H28	126.52	126.8	C3-C4-H28	109.860	109.7	C2-C16-C17	126.377	126.377
O19-C18-H33	115.82	–	C11-C12-O13	110.68	110.7	C3-C4-H29	109.914	109.7	C2-C16-H36	117.000	117.000
C15-O19-C18	107.40	–	C11-C12-H29	133.34	124.7	C5-C4-H28	109.756	109.7	C17-C16-H36	116.585	116.585
C2-C3-C4	111.42	112.3	O13-C12-H29	115.97	124.7	C5-C4-H29	110.122	109.7	C16-C17-C18	123.418	123.418
C2-C3-H20	109.43	–	C9-O13-C12	107.73	107.98	H28-C4-H29	107.060	108.2	C16-C17-C22	120.581	120.581
C2-C3-H21	110.20	–	C2-C14-C15	131.05	–	C4-C5-C6	111.819	111.02	C18-C17-C22	115.940	115.940
C4-C3-H20	108.91	–	C2-C14-H30	115.36	–	C4-C5-H30	108.575	109.4	C17-C18-C19	122.449	122.449
C4-C3-H21	110.73	–	C15-C14-H30	113.59	–	C4-C5-H31	110.956	109.4	C17-C18-Cl24	119.941	119.941
H20-C3-H21	106.00	–	C14-C15-C16	129.62	–	C6-C5-H30	109.078	109.4	C19-C18-Cl24	117.597	117.597
C3-C4-C5	110.92	111.5	C14-C15-O19	121.65	–	C6-C5-H31	109.949	109.4	C18-C19-C20	119.428	119.428
C3-C4-H22	110.06	109.3	C16-C15-O19	108.72	–	H30-C5-H31	106.284	108.0	C18-C19-H37	119.555	119.555
C3-C4-H23	109.43	109.3				C1-C6-C5	119.114	118.23	C20-C19-H37	121.015	121.015
C5-C4-H22	109.83	109.3				C1-C6-C7	115.970	118.29	C19-C20-C21	120.228	120.228
C5-C4-H23	109.61	109.3				C5-C6-C7	124.860	123.35	C19-C20-H38	119.865	119.865
H22-C4-H23	106.90	108.0				C6-C7-C8	127.063	123.77	C21-C20-H38	119.906	119.906
C4-C5-C6	112.69	112.3				C6-C7-H32	116.679	118.1	C20-C21-C22	119.142	119.142
C4-C5-H24	108.99	109.1				C8-C7-H32	116.190	118.1	C20-C21-H39	121.160	121.160
C4-C5-H25	109.89	109.1				C7-C8-C9	120.118	121.93	C22-C21-H39	119.698	119.698
C6-C5-H24	109.62	109.1				C7-C8-C13	124.075	122.2	C17-C22-C21	122.805	122.805
C6-C5-H25	109.31	109.1				C9-C8-C13	115.746	115.85	C17-C22-Cl23	118.915	118.915
H24-C6-H25	106.12	107.9				C8-C9-C10	122.906	122.94	C21-C22-Cl23	118.279	118.279
C1-C6-C5	120.30	119.5				C8-C9-Cl15	119.023	118.34			

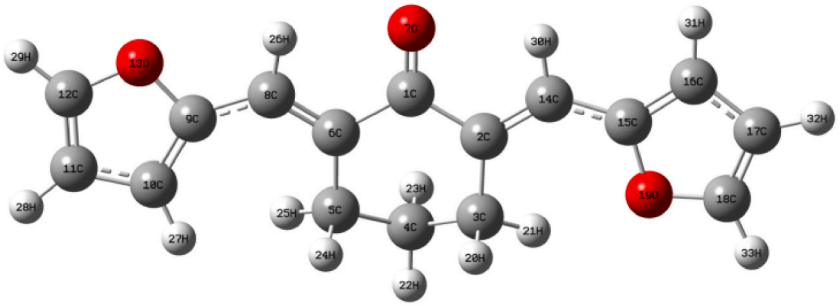

Fig. 3. Molecular structure of DFC.

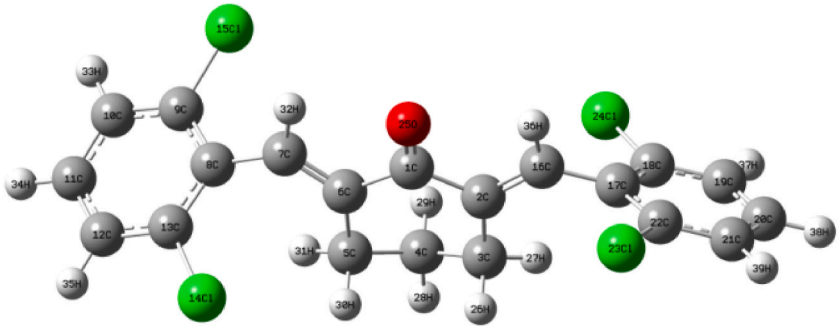

Fig. 4. Molecular structure of DCC.

Table 6
The Second order Fock-matrix natural bond orbital analysis of DFC and DCC molecules.

Type	DFC					DCC				
	Donor (i)	ED/e	Acceptor (j)	ED/e	$E^{(2)}$ kcal/mol	Donor (i)	ED/e	Acceptor (j)	ED/e	$E^{(2)}$ kcal/mol
π-π*	C3-C10	1.81480	C4-O17	0.24483	20.33	C3-C10	1.86298	C4-O17	0.18598	18.28
			C 26-C27	0.33498	14.98					
π-π*	C5-C12	1.81480	C4-O17	0.24483	20.33	C5-C12	1.86298	C4-O17	0.18598	18.28
			C18-C19	0.33498	14.98					
π-π*	C18-C19	1.77991	C5-C12	0.15772	15.23	C18-C20	1.66692	C19-C21	0.37861	18.51
			C21-C23	0.27383	16.63			C22-C23	0.32794	19.25
π-π*	C26-C27	1.77991	C 3-C10	0.15772	15.23	C19-C21	1.68340	C18-C20	0.41393	19.70
			C29-C31	0.27383	16.63			C22-C23	0.32794	19.01
π-π*	C21-C23	1.83203	C18-C19	0.33498	15.99	C22-C23	1.66217	C18-C20	0.41393	21.05
π-π*	C29-C31	1.83203	C26-C27	0.33498	15.99			C19-C21	0.37861	20.97
π-π*						C27-C29	1.66692	C28-C30	0.37861	18.51
								C31-C32	0.32794	19.25
π-π*						C28-C30	1.68340	C27-C29	0.41393	19.70
								C31-C32	0.32794	19.01
π-π*						C31-C32	1.66217	C27-C29	0.41393	21.05
								C28-C30	0.37861	20.97
n-α*						O17	1.87682	C3-C4	0.06679	19.71
								C4-C5	0.06679	19.71

$E^{(2)}$ – Conjugative energy; ED-electron density.

hydrogen atoms at C6, C1, and C2 reduces the Cyclohexanone structure to half chair. Aberration of the angles C3-C2-C14, C2-C14-C15, C14-C15-C16, C5-C6-C8, C6-C8-C9, C8-C9-C10 are about 125.37°, 131.05°, 129.62°, 123.84°, 128.90° and 137.00°, respectively, have reduced from the normal values due to the steric repulsion. Unlike other Cyclohexanone derivatives, calculated values indicates that the ring Phenyl ring1 (C2-C14-C15-O19 = −3.00) and Phenyl ring2 (C6-C8-C9-C10 = 9.28) are nearly planar with the central Cyclohexanone ring.

3.2. Vibrational spectral analysis

The vibrational behaviour of DFC and DCC molecules was analyzed using FT-IR and FT-Raman spectroscopy in the visible range

(4000-400 cm^{-1}), with the recorded wavenumbers included in Tables S1 and S2 for DFC and DCC, respectively. Further, Vibrational wave numbers were calculated using DFT based hybrid pople basis set B3LYP/6-311G(d,p) level. It means that 6 Gaussian type orbitals (GTOs) for the core orbital (K), 3 GTOs for inner valence (L), 2 different GTOs for outer valence (MG). These basis sets usually applied for organic molecules, often said to be double zeta (2 functions per atomic orbitals) or triple zeta, it can be denoted as K-LMG (6–311), i.e., K is number of sp-type inner shell GTOs, L is number of inner valence s – and p –type GTOs, M is number of outer valence s – and p-type GTOs and G indicates that GTOs are used. The recorded FT-IR and simulated IR spectra of both DFC and DCC are shown in Fig. 5a-b and 5(c-d), respectively. Similarly, the FT-Raman and simulated Raman spectra are shown in Fig. 6a-b and 6(c-d) for both DFC and DCC, respectively. To estimate the calculated wavenumber with recoded the scaling factor 0.967 was used [47].

3.2.1. C–H vibrations

The C–H vibrations in DFC and DCC molecules manifest in distinct ranges. The C–H stretching vibrations typically occur between 3100 and 2879 cm^{-1} [48,49] in the aromatic heterocyclic ring. In DFC, the C-H stretching, computed at 3170, 3168, 3164, 3147,3138 cm^{-1} (mode nos. 1–5) as a pure mode with TED contribution of 99 %. The same vibrations are recorded in FT-IR and FT-Raman at 3170, 3168, 3164, 3147, 3139 cm^{-1} and 3171, 3169, 3165, 3148, 3138 cm^{-1}. Whereas, in DCC, C-H vibration computed at 3105, 3103, 3101, 3099, 3080, 3078 cm^{-1} (mode nos. 1–6) as a pure mode as shown in Table S2. There seems a lowering of vibrational (νC-H) wave number, it is due to increasing in total energy (−2678.3054 a.u) of this molecule.

The in-plane and out-of-plane bending modes of C-H for DFC and DCC molecules are typically observed to be highly associated with other vibrations, appearing in the ranges of 1300-1000 cm^{-1} and 1000-750 cm^{-1}, respectively [48,49]. In DFC, the computed ipb C-H band are obtained at 1231 (1232(FT-IR), 1233(FT-Raman)), 1199 (1199, 1200), 1167 (1168, 1169), 1144 (1145, 1146), 1101 (1101, 1101), 1068 (1068, 1069) cm^{-1} (mode nos. 35–38, 42, 44) using B3LYP/6-311G (d, p) level of basis set. These computed values are well coincided with recorded FT-IR and FT-Raman spectra. For DCC, the ipb C-H also appeared as a mixed mode of with νC-C vibrations. The aromatic C–H out-of-plane bending vibrations in DFC and DCC molecules are good correlated recorded as well as computed values.

3.2.2. CH_2 group vibrations

The study reveals, the vibrations caused by uneven stretching for Methylene (CH_2) group appear around 3000-2920 cm^{-1},

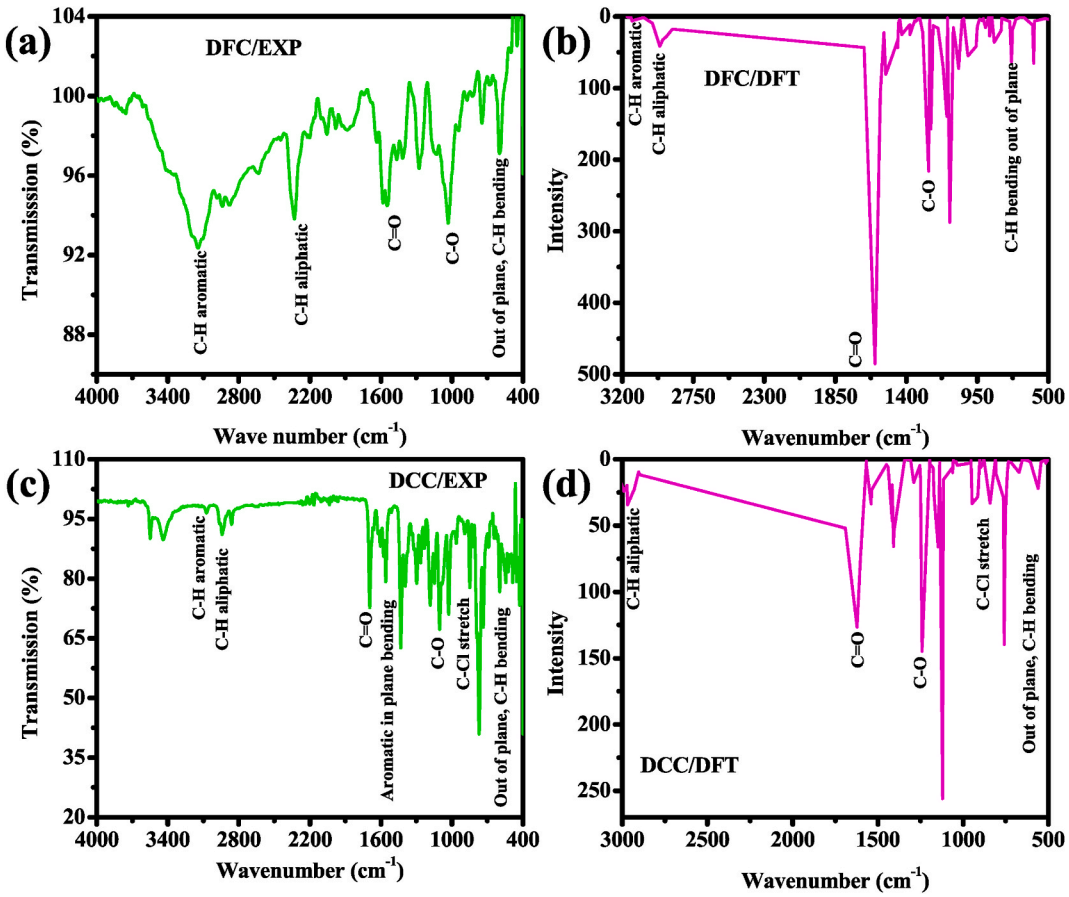

Fig. 5. Experimental and theoretical comparison of FTIR spectra of DFC (a & b) and DCC(c &d).

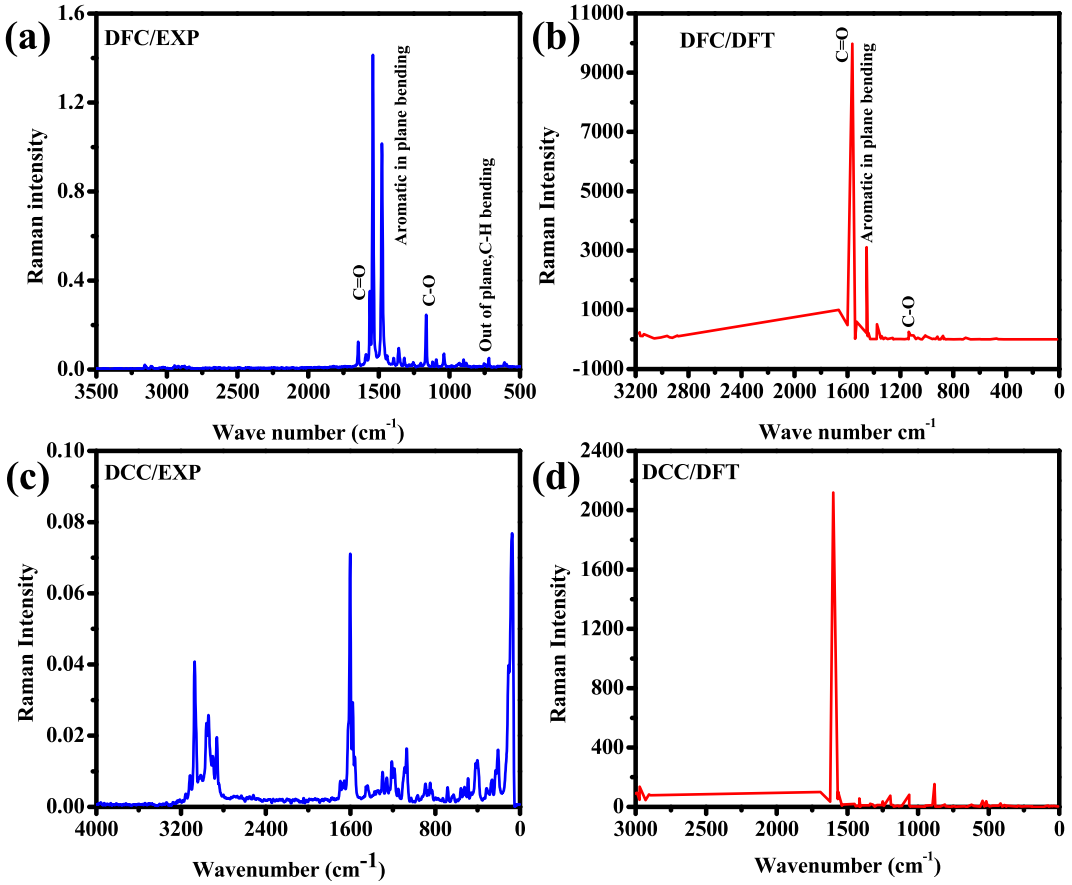

Fig. 6. Experimental and theoretical comparison of FT-Raman spectra of DFC (a & b) and DCC (c &d).

whilemethylene(CH_2) symmetrical stretching falls between 2900-2800cm^{-1}[50,51]. In DFC the νCH_2, stretching recorded at 2884, 2879 cm^{-1} in FT-IR and 2885, 2878 cm^{-1}in FT-Raman, whereas the calculated wavenumbers at 2884 and 2878 cm^{-1} (mode nos.13 and14).The $\nu_{asy}CH_2$ stretching in DFC recorded at 2964, 2944, 2941 cm^{-1} by Infrared Fourier Transform and 2964, 2945, 2922 cm^{-1} using Raman spectrum. Similarly, the calculated values are coincided well with the recorded one. The ν_{asy} CH_2 in DFC recorded at 2964, 2944 and 2941 cm^{-1} using FT-IR, whereas, FT-Raman recorded at 2964, 2945 and 2922 cm^{-1}, the calculated wavenumber for same mode are in the ranges of 2963, 2944 and 2921 cm^{-1} (mode no: 10, 11 and 12). The ν_{sym} $CH_2$and ν_{asy} CH_2 stretching vibrations wavenumber in DCC molecule are appeared as higher than that of DFC in both recorded and calculated (mode nos. 8–11). It is due to the less energy distributed over methylene group. These calculated wavenumbers ~94–99 % contributes to this mode of vibrations.

It is familiarly known that, CH_2group bending vibrations are in the range between 1668 and 858 cm^{-1}, scissoring as a medium intense FT-IR band [52]. In DFC, frequencies 1442, 1430 and 1441, 1431 cm^{-1} are assigned to scissoring and are recorded by FT-IR and FT-Raman respectively, whereas the calculated wavenumber at 1441 and 1429 cm^{-1} are coincides well with the recorded results. The computed wavenumber at1379-1342 cm^{-1} (mode nos.25-28) were assigned to CH_2 group wagging vibration, it supports well with the recorded values. The twisting of CH_2 occurs at 1199 (FT-IR) and at 1200 cm^{-1} (FT-Raman). On the other hand, the ipb and opb vibrations in DCC are appeared as almost same results in both recorded and computed.

3.2.3. C=O vibrations

The C=O bond exhibits considerable strength owing to a significant alteration in molecular dipole orientation and minimal interference from other vibrational modes. The significant alteration in the molecular dipole orientation between carbonyl carbon and oxygen in all compounds is characterized by a high-intensity, abrupt peak in the range of 1688-1454 cm^{-1} [40]. In the DFC compound, the C_3=O_{14} stretching vibrations are observed in FT-IR and FT-Raman spectra at 1668 cm^{-1} as a medium strong band. The calculated value is 1667 cm^{-1} (mode no. 15) with a TED contribution of 48 % [53]. The DCC molecule exhibits a C=O stretching band at 1691 cm^{-1} in the FT-IR spectrum and at 1692 cm^{-1} in the FT-Raman spectrum. The calculated wavenumber for this mode is 1691 cm^{-1} (mode no. 15) with a TED contribution of 34 %. The vibration of the carbonyl group demonstrates great concordance with one another and aligns with the literature [53].

3.2.4. C-Cl vibrations

The C-Cl stretching vibration for the DCC molecule is generally falls in the region 730-580 cm^{-1}[54].The wavenumber computed at 753 and 394 cm^{-1}(mode nos.68 and 87) are assigned to C-Cl stretching mode, the recorded wavenumber appeared in Infrared Fourier Transform and Raman spectrumat 753 and 394 cm^{-1} respectively, with the TED contribution of ~20 %. The lowering of computed and recorded wavenumber may be due to presence of other rings in the molecular system.

3.2.5. Vibrations with in a ring

The fragrant ring within the structure is indicated by C–C and C═C stretching vibrations, with the anticipated carbon–carbon stretching vibrations occurring between 1625 and 1430 cm^{-1}, as reported by Varsanyi [48,55]. Additionally, C–C stretching bands of varying intensities are present in the ranges of 1668–1454, 1380–1378, 1259–1245, 1199–1168, and 1124–1068 cm^{-1}. In DFC, the wave numbers calculated are 1667, 1599, 1564, 1542, 1530, 1455, 1379-1125, and 959-799 cm^{-1} (mode nos. 15, 16, 17, 18, 19, 20, 25, 41, and 49–61) for both ring systems. In the FT-IR spectrum, the wavenumbers 858, 844, and 800 cm^{-1} correspond to the stretching mode of C–C vibrations. The bands corresponding to C–C stretching observed in the FT-Raman spectrum are located at 858, 843, 799, 797, and 739 cm^{-1}. The same vibrations in the DCC molecule were calculated at 1622, 1568, 1567, 1539, 1538, 1416, 1416, 1339, 1252, 1250, 1196, and 1192 cm^{-1} (mode numbers 16, 18–21, 25, 26, 30, 35, 36, 38, 39) as a mixed mode. The C–H ipb, CH_2 wagging, and torsional vibrations occur at elevated wave numbers relative toout-of-planebending. In the DFC molecule, the bands seen at 588, 522, 474, 460, and 422 cm^{-1} in FT-IR are attributed to the C–C–C deformation bending vibrations of the phenyl group and the five-membered cyclopentanone. The C–C–C vibrations in the FT-Raman spectrum occur at 588, 523, 475, 459, and 423 cm^{-1}. The theoretically calculated values are 587, 521, 473, 459, and 421 cm^{-1} (mode numbers 74, 75–78). The C-C-C deformation vibrations in the DCC molecule align well with the observed and computed values of the DFC.

3.2.6. UV–Vis Spectra and electronic properties

To explore the electronic shift in DFC and DCC molecules, the UV–Visible spectra were recorded, excitation wavelengths were compared with computed TD-DFT results, also analyzed different excitation in both molecules [55] and IEF-PCM [56] calculations were computed in both gas and acetone phase for DFC molecule, and gas and chloroform phase for DCC molecule, results obtained are listed in Tables 7 and 8. The experimental and stimulated UV–Vis spectra of DFC (Fig. 7a and b) and DCC (Fig. 7c and d), was obtained in an ethanol solution. Acetone and chloroform are utilized as solvents for the compounds due to their minimal effect in UV–Vis microscopy.

Analysis using the UV–Vis spectra for both DFC and DCC reveals two prominent bands at 432 nm and 285 nm, indicative of the n→π* shift. The electronic shift designation for the initial transition is n→π* i.e. nonbonding (n) electron pair to anti-bonding (π*) orbital. This type of transition usually weaker appears in unsaturated molecules containing oxygen and nitrogen. Moreover, the carbonyl compound having double bonds and two or more single bonds exhibits n→π* transition in the ranges of 300–350nm. In the presence of aldehydes and ketones, n→π* transition arises from lone pair (n) of electrons in $2p_y$ orbitals of oxygen atom into the anti-bonding (π*) orbital of the carbonyl group. Further, the compound containing hetero atoms, exhibit excitation band at above the 300nm. The n→π* transition indicates that it is weaker interaction, although it consists of carbonyl group and hetero atoms, and hence this transition exhibits above the 432nm, in addition the conjugation C=C-C-C=O and C=C-O=C are twice in DFC and hence it possesses nearly eight double bonds, thus it emits the colours in the visible range (λ_{max} = 432nm). As a result, it has the band gap around 2.870eV. The formation of the system results in a deficiency of electrons, while the π* system acquires an additional electron to stabilize the π* orbital [57]. The TD-DFT results also show a meaningful excitation wavelength between occupied and unoccupied orbitals at the first excited state, say, HOMO and LUMO is about 406.27 nm and 404 nm (~3.0538eV) in gas phase and acetone solvent respectively. Similarly, the excited state 2 show the transition (n→π*) at 381 and 388.61 nm (~3.2288eV), and excited 3 show the transitions at 353.66 and 363.55nm (~3.4925eV) respectively.

Frontier Molecular Orbital (FMO) electron density explains the reactive site of π electron density in the delocalized conjugated system for DFC and DCC [58]. The HOMO-LUMO is found to be small for both the molecules due to conjugated system which leads to large possibility for inter molecular charge transfer from electron donor group to electron acceptor group through π conjugated system [59]. The HOMO and LUMO energy are 3.53 eV and 4.49 eV. The Homo and Lumo pictorial representation of DFC and DCC have shown in Fig. 8a and b, respectively.

The energy gap between the i.e. (HOMO-LUMO energy gap) DFC and DCC provide the bioactivity property through intramolecular charge transfer [60,61]. The maximum absorption wavelength assigned to DFC molecule the possible transition from HOMO-2→LUMO (100 %), HOMO-2→LUMO (97 %) and HOMO-1→LUMO (95 %). Similarly for the DCC molecule the possible transition from HOMO-4→LUMO (42 %), HOMO-1→LUMO (93 %), HOMO-3→LUMO (87 %).

3.3. Molecular docking

Molecular docking plays a vital role in finding binding mode of ligand molecule for target protein. Here, glide module was used to perform the docking studies. The validation of docking tool was done by re-docking procedure. The co-crystallized compound (DTQ) retrieved and re-docked in protein active site. The superposition of co-crystallized and re-docked pose illustrated in Fig. 9. The RMSD value 2 will be acceptable range, here, obtained value is 0.34, and hence docking protocol was used for further studies [40]. The well known ligand of CDK2 is BMS265246 [38], since inhibition of CDK2 expression will be evidenced for rectification of various colon cancer cell lines. Thus, reference ligand and two synthesized compounds were docked using same protocol used for re-docking. All the three compounds obtained the glide score value of −6.327, −6.888 (DFC) and −5.972 (DCC), respectively. Pyridine nitrogen of

Table 7
Experimental and Calculated absorption wavelength and oscillator strengths of DCC using the TD-DFT method at B3LYP/6-311G(d,p) method.

DFT/B3LYP									Results	
Excitation	Wavelength λ (nm) Gas Phase	Oscillator Strength (f)	CI Expansion Co efficient	Excitation	Wavelength λ (nm) Acetone Phase	Oscillator Strength (f)	CI Expansion Co efficient	Experimental (nm)	Assignment	In Solvent [a]Major Contribution (≥10 %)
Excited State 1	406.27	0.0000	0.69842	67 → 68	404.10	1.1078	0.70657	432	n→π*	H→L (100 %)
Excited State 2	381.22	0.9112	0.70471	65 → 68	388.81	0.0000	0.69665	–	n→ π *	H-2→LUMO (97 %)
Excited State 3	353.66	0.0044	0.68235	66 → 68	363.55	0.0081	0.68862	–	n→ π *	H-1→LUMO (95 %)
	–	–	−0.17811	67 → 69	–	–	−0.14190	–		

(H-HOMO; L-LUMO).

Table 8
Experimental and calculated absorption wavelength and oscillator strengths of DCC using the TD-DFT method at B3LYP/6-311G(d,p) method.

DFT/B3LYP								Results		
Excitation	Wavelength λ (nm) Gas Phase Phase	Oscillator Strength (f)	CI Expansion Co efficient	Excitation	Wavelength λ (nm) Chloroform Phase	Oscillator Strength (f)	CI Expansion Co efficient	Experimental (nm)	Assignment	In Solvent [a]Major Contribution (≥10 %)
Excited State 1	388.63	0.0021		**Excited State 1**	380.88	0.0037		285	n→π*	H-4→L (42 %), H→L (52 %)
Excited State 2	303.19	0.4046		**Excited State 2**	312.39	0.4961			n→ π *	H-1→L (93 %)
Excited State 3	298.03	0.0101		**Excited State 3**	306.17	0.0133			n→ π *	H-3→L (87 %)

(H-Homo, L-Lumo).

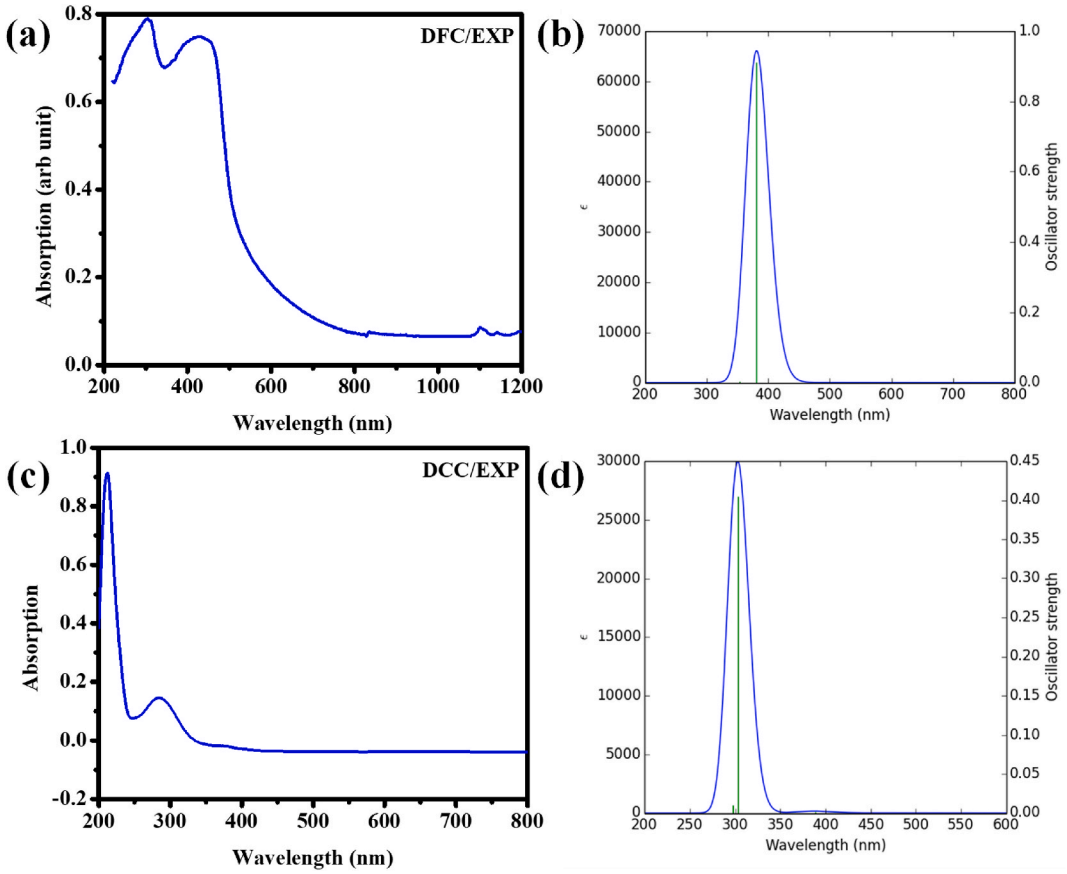

Fig. 7. Experimental and theoretical UV–Vis Spectra of DFC (a &b) and DCC (c &d).

reference molecule accepting one electron from LYS33 formed a hydrogen bond interaction (Fig. 10a and b). Vander Walls and polar interaction formed by fluorine atom with GLY13, GLU12, GLY11, ILE10, and ASP132, and GLN131, respectively. Carbonyl oxygen of DFC showed the hydrogen bond interaction with LEU83 (Fig. 11a and b). DCC molecule confirms its position in active site by forming hydrogen bond interaction with LEU33. Both chlorine atom of DCC molecule formed the hydrophobic interaction with ILE10, VAL18, PHE80, PHE82, LEU83, VAL64, stabilized its position illustrates in (Fig. 12a and b). Based on the above studies, our compound is suitable selection for the further process. Consequently, we took into the in-vitro studies.

3.4. Drug likeliness

Lipinski rule of five is tested for the DFC and DCC by using Qikprop in Schrödinger maestro and their results are tabulated in Table 9.On comparing the values of the compounds DFC and DCC with the permissible values, Molecular weights are less than the permissible values of 130–725. Donor Hydrogen bond is between permissible (0–6). Acceptor hydrogen bonds are between (2.0–6.0). Total Solvent Accessible Surface Area is between the permissible (300–1000°A). Predicted octanol/water partition co-efficient is between permissible −2.0 to 6.5.Predicted brain/blood partition coefficient is between the permissible value of −3.0 to 1.2.Predicted aqueous solubility is between −6.5 and 0.5. Human oral absorption is 3 which are good. On considering these values the molecules are exhibiting good drug ability.

3.5. Cell proliferation (MTT) assay

The MTT assay is used to determine how much the chemicals have proliferated the cells in comparison to the control group. We bought DMSO and 3-(4,5-dimethylthiazol-2-yl)-2, 5-diphenyltetrazoliumbromide (MTT) from Sigma Aldrich. 5 × 103 HCT116 cells were put into each well of the 96-well plate. The cells were treated with varying amounts of DFC and DCC the following day, and they were then incubated for a further 48 hours. Each well receives an addition of freshly made MTT following the incubation time. The cells underwent a 4-h incubation period at 37 °C. DMSO is added to the formed formazan crystals to solubilize them. At 570 nm, the absorbance is measured with a plate reader.

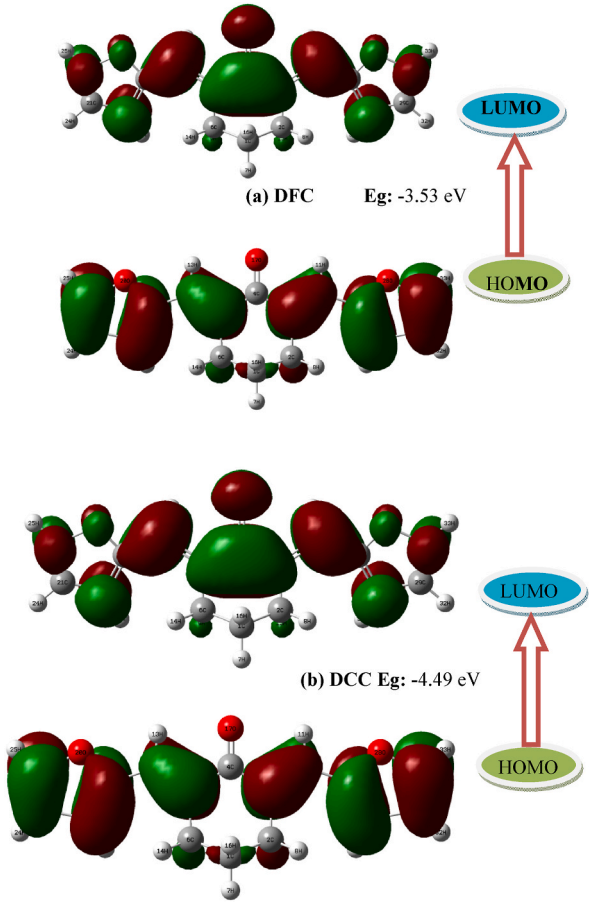

Fig. 8. The Homo and Lumo pictorial representation of (a) DFC and (b) DCC.

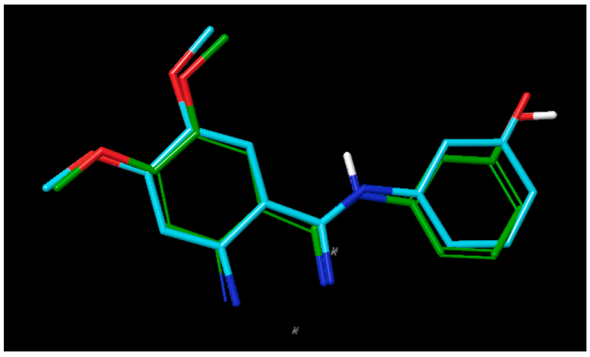

Fig. 9. Superposition of inhibitor compound with its crystal structure (1DI8), color coded GLIDE prediction Green and bound Cyan (Color figure online). (For interpretation of the references to color in this figure legend, the reader is referred to the Web version of this article.)

3.6. Reduced colon cancer cell proliferation

The following compounds DFC and DCC were used to check their anticancer effects on HCT-116 colon cancer cells. These compounds show good binding energy with the androgen receptors. Colon cancer cells have androgen receptors and its activation has triggered apoptotic responses in *in-vitro* and *in-vivo* conditions (R) MTT assay with DFC and DCC on colon cancer cells showed a reduced cell proliferation rate. Anticancer effects were seen for the duration of 48 hrs.,with different concentration ranges from 20, 40, 80, and 120 μM. It is seen that the percentage of proliferative cells decreases as the concentration of the compounds increases as seen in the graph (Fig. 13). Followed by which concentration of the compounds which killed half the population of cells (IC_{50}) were calculated

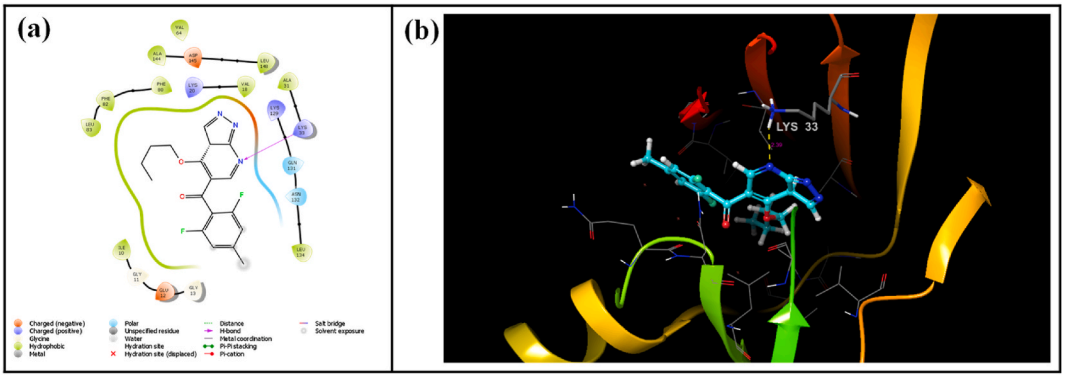

Fig. 10. Molecular interaction of BMS265246with catalytically important residues, a) 2-dimensional ligand receptor interaction of BMS265246 inside protein packet, b) 3-dimensional disposition of BMS265246 with vital residues.

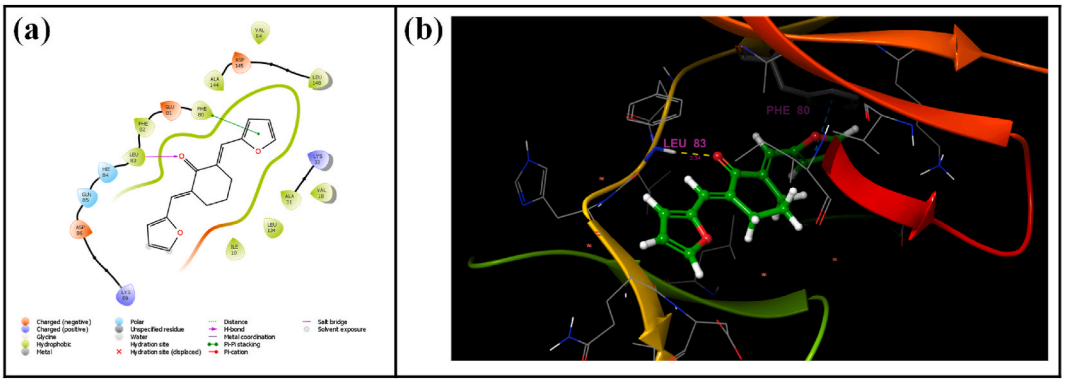

Fig. 11. Molecular interaction of DFC with catalytically important residues, a) 2-dimensional ligand receptor interaction of DFC inside protein packet, b) 3-dimensional disposition of DFC with vital residues.

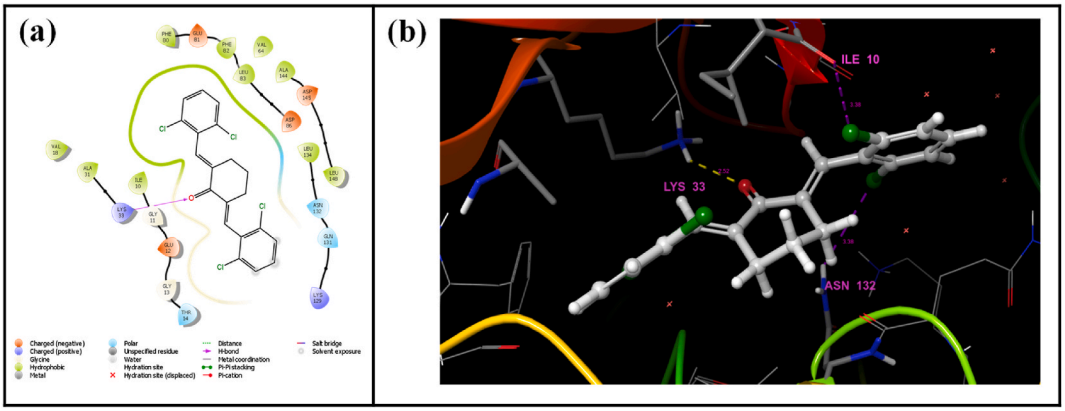

Fig. 12. Molecular interaction of DCC with catalytically important residues, a) 2-dimensional ligand receptor interaction of DCC inside protein packet, b) 3-dimensional disposition of DCC with vital residues.

Table 9
Results of Lipinski rule of five for the compounds DFC and DCC.

Compound Name	MW	Donors HB	Acceptors HB	SASA	Qplog P_0/w	QPlog BB	QPlogS	%Human Oral Absorption
DFC	254.285	0	3	433.369	2.809	0.087	−2.208	3
DCC	412.142	0	2	478.128	4.264	0.585	−4.709	3

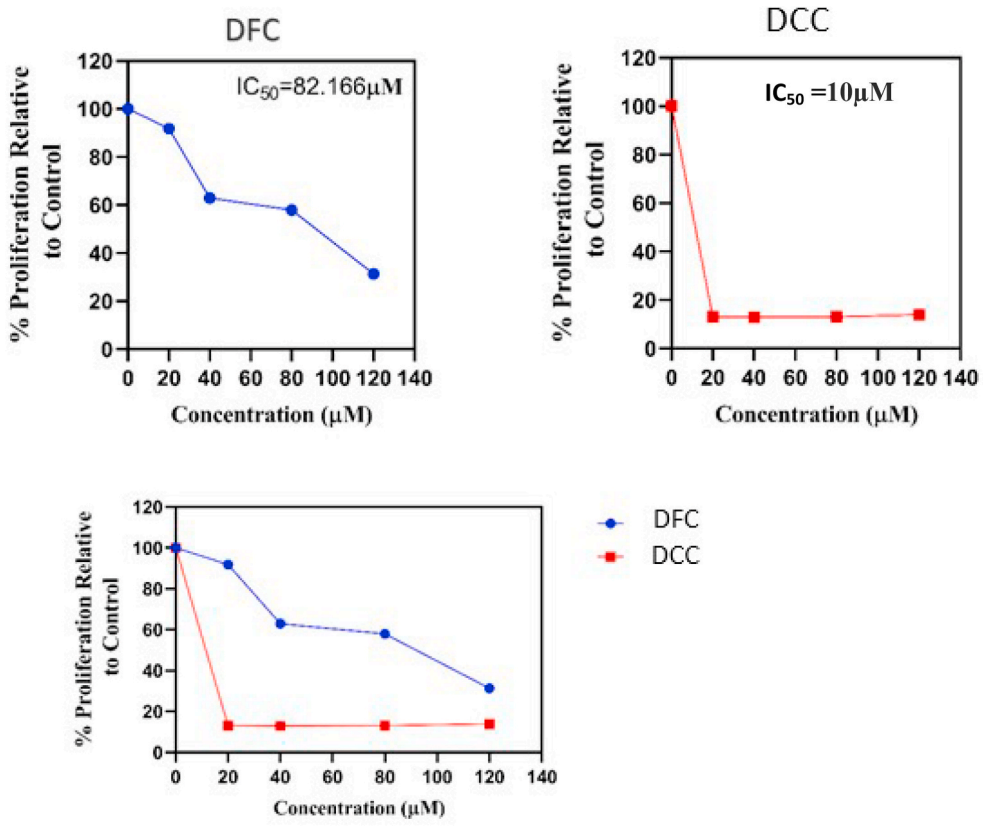

Fig. 13. Effects of DFC and DCC on proliferation of human colon cancer cells of HCT -116.

from the proliferation graph. The IC_{50} for the compounds was found to be 82.16μM and around 10μM for DFC and DCC [38]. These compounds have shown the potency to inhibit colon cancer growth *in-vitro* and can be studied further for therapeutic purposes.

4. Conclusion

The molecules DFC and DCC were synthesized and their lattice characteristics were analyzed using XRD and DFT methods. The molecular geometry revealed twisted boat confirmation with puckering angle 59.7 (4)° and 64.4 (3)° due to steric effects and phase angle explores symmetrical puckering in these compounds. The results obtained in both experimental and computational computations, and which are closely matched the information found in existing literature. The functional groups of the produced compounds were analyzed using FTIR and FT-Raman spectroscopy. The obtained values were then compared with the hybrid B3LYP level of theory. The results appear to be in good accord with the calculated values. The electronic transitions of n-π* were investigated using UV–Visible spectroscopy, with the wavelength cut-offs observed at 432nm and 285nm. The transition from the ground state to the excited state (n→π*) of the DFC molecule emits blue light in the visible spectrum, with a maximum wavelength of 432 nm. The band gap in DFC is −3.53eV, which is smaller due to its larger concentration of conjugative bonds. On the other hand, the band gap in DCC is 4.49eV, making it significantly higher compared to DFC. The drug likeness was assessed using the Lipinski rule, and the result indicates that DFC and DCC are highly suited for drug likeliness. In addition, the interaction with macromolecules was investigated through molecular docking using the Glide tool, which is included into the Maestro Schrodinger software. The docking investigation revealed that both drugs exhibited strong interactions with critical residues in the active site and occupied the site with a favourable conformation. Therefore, both chemicals were included in the CRC investigation due to their ability to effectively suppress the growth of colon cancer cells in an in-vitro environment. Based on the outcome, we highly recommend conducting additional research as both drugs demonstrate anti-cancer effectiveness.

Data and code availability

The single crystal crystallographic data can be accessed in the Cambridge Structural Database (CSD) using the following database IDs: (i) ID: XOZWOZ, CCDC: 758293 for the DFC molecule and ID: LAPROL, CCDC: 872542 for the DCC molecule. The crystallographic CIF data of DFC and DCC are included in supplementary material, there is no code available.

CRediT authorship contribution statement

S. Sathiyamoorthi: Writing – original draft, Resources. **Meganathan Chandrasekaran:** Writing – original draft, Validation, Project administration. **K. Thiruppathi:** Resources. **P. Padmanathan:** Validation, Investigation. **S. Subashchandrabose:** Investigation, Data curation. **S. Gomathi:** Investigation, Formal analysis.

Declaration of competing interest

The authors declare the following financial interests/personal relationships which may be considered as potential competing interests:Meganathan C reports administrative support was provided by Sri Sai Ram Engineering College. Meganathan C reports a relationship with Sri Sai Ram Engineering College that includes: employment. If there are other authors, they declare that they have no known competing financial interests or personal relationships that could have appeared to influence the work reported in this paper.

Acknowledgement

The authors thank Professor S Kabilan Annamalai University, Chidambaram for use of the Schrodinger software Facility for docking.

Appendix A. Supplementary data

Supplementary data to this article can be found online at https://doi.org/10.1016/j.heliyon.2024.e38300.

References

[1] Ossama Daoui, Mohamed Bakhouch SouadElkhattabi, Salah Belaidi, Richie R. Bhandare, Afzal B. Shaik, Suraj N. Mali, Samir Chtita, Cyclohexane-1,3-dione derivatives as future therapeutic agents for NSCLC: QSAR modeling, in silico ADME-tox properties, and structure-based drug designing approach, ACS Omega 8 (2023) 4294–4319, https://doi.org/10.1021/acsomega.2c07585.

[2] R.J. Pagliero, S. Lusvarghi, A.B. Pierini, R. Brun, M.R. Mazzieri, Synthesis, stereoelectronic characterization and antiparasitic activity of new 1-benzenesulfonyl-2-methyl-1, 2, 3, 4-tetrahydroquinolines, Bioorg. Med. Chem. 18 (2010) 142–150, https://doi.org/10.1016/j.bmc.2009.11.010.

[3] S.-F. Barbuceanu, G. Saramet, G.L. Almajan, C. Draghici, F. Barbuceanu, G. Bancescu, New heterocyclic compounds from 1,2,4-triazole and 1,3,4-thiadiazole class bearing diphenylsulfone moieties. Synthesis, characterization and antimicrobial activity evaluation, Eur. J. Med. Chem. 49 (2012) 417–423, https://doi.org/10.1016/j.ejmech.2012.01.031.

[4] M. Gumus, M. Yakan, I. Koca, Recent advances of thiazole hybrids in biological applications, Future Med. Chem. 11 (2019) 1979–1998, https://doi.org/10.4155/fmc-2018-0196.

[5] A.E.-G.E. Amr, M.H. Sherif, M.G. Assy, M.A. Al-Omar, I. Antiarrhythmic Ragab, Serotonin antagonist and antianxiety activities of novel substituted thiophene derivatives synthesized from 2-amino-4, 5, 6, 7-tetrahydro-N-phenylbenzo [b] thiophene3-carboxamide, Eur. J. Med. Chem. 45 (2010) 5935–5942, https://doi.org/10.1016/j.ejmech.2010.09.059.

[6] R.M. Mohareb, Y.R. Milad, A.A. Masoud, New approaches for the synthesis of heterocyclic compounds derived from cyclohexan-1, 3-dione with anti-proliferative activities, Acta Chim. Slov. 68 (2021) 72–87. PMID: 34057521.

[7] T. Anwar, P. Kumar, A.U. Khan, Modern tools and techniques in computer-aided drug design, in: Molecular Docking for Computer-Aided Drug Design, Elsevier, 2021, pp. 1–30, https://doi.org/10.1016/B978-0-12-822312-3.00011-4.

[8] J. Tsemeugne, E.S. Fondjo, J. Tamokou, T. Rohand, A.D. Ngongang, J.R. Kuiate, B.L. Sondengam, Synthesis, characterization, and antimicrobial activity of a novel trisazo dye from 3- amino-4H-thieno [3,4-c][1]benzopyran-4-one, International Journal of Medicinal Chemistry 2 (2018) 1–8, https://doi.org/10.1155/2018/9197821, 2018.

[9] K. Bielawski, K. Leszczyńska, Z. Kałuża, A. Bielawska, O. Michalak, T. Daniluk, O. Staszewska-Krajewska, A. Czajkowska, N. Pawłowska, A. Gornowicz, Synthesis and antimicrobial activity of chiral quaternary N-spiro ammonium bromides with 3′,4′-dihydro-1′h-spiro[isoindoline-2,2′isoquinoline] skeleton. Drug Design, Development and Therapy 11 (2017) 2015–2028, https://doi.org/10.2147/DDDT.S133250.

[10] Sariya Mapoung, et al., Cyclohexanone curcumin analogs inhibit the progression of castration-resistant prostate cancer in vitro and in vivo 110 (2) (2019) 596–607, https://doi.org/10.1111/cas.13897.

[11] L. Li, F.S. Braiteh, R. Kurzrock, Liposome-encapsulated curcumin: in vitro and in vivo effects on proliferation, apoptosis, signaling, and angiogenesis, Cancer 104 (2005) 1322–1331, https://doi.org/10.1002/cncr.21300.

[12] P. Anand, H.B. Nair, B. Sung, A.B. Kunnumakkara, V.R. Yadav, R.R. Tekmal, B.B. Aggarwal, Design of curcumin-loaded PLGA nanoparticles formulation with enhanced cellular uptake, and increased bioactivity in vitro and superior bioavailability in vivo, Biochem. Pharmacol. 79 (2009) 330–338, https://doi.org/10.1016/j.bcp.2009.09.003.

[13] G. Shoba, D. Joy, T. Joseph, M. Majeed, R. Rajendran, P.S. Srinivas, Influence of piperine on pharmacokinetics of curcumin in animals and human volunteers, Planta Med. 64 (1998) 353–356, https://doi.org/10.1055/s-2006-957450.

[14] P. Anand, S.G. Thomas, A.B. Kunnumakkara, C. Sundaram, K.B. Harikumar, B. Sung, S.T. Tharakan, K. Misra, I.K. Priyadarsini, K.N. Rajasekharan, et al., Biological activities of curcumin and its analogues (congeners) made by man and mother nature, Biochem. Pharmacol. 76 (2008) 1590–1611, https://doi.org/10.1016/j.bcp.2008.08.008.

[15] S. Gafne, S.K. Lee, M. Cuendet, S. Barthelemy, L. Vergnes, S. Labidalle, R.G. Mehta, C.W. Boone, J.M. Pezzuto, Biologic evaluation of curcumin and structural derivatives in cancer chemoprevention model systems, Phytochemistry65 (2004) 2849–2859, https://doi.org/10.1016/j.phytochem.2004.08.008.

[16] Yu Zhao Lee, et al., Development and validation of a bioanalytical method for quantification of 2,6-Bis-(4-hydroxy-3-methoxybenzylidene)- cyclohexanone (BHMC) in rat plasma, Molecules 17 (2012) 14555–14564, https://doi.org/10.3390/molecules171214555.

[17] Cyclohexane and its functionally substituted derivatives: important class of organic compounds with potential antimicrobial activities, J Microbiol Biotech Food Sci 9 (1) (2019) 84–87, https://doi.org/10.15414/jmbfs.2019.9.1.84-87.

[18] S. Mapoung, P. Pitchakarn, S. Yodkeeree, C. Ovatlarnporn, N. Sakorn, P. Limtrakul, Chemosensitizing effects of synthetic curcuminanalogs on human multi-drug resistance leukemic cells, Chem. Biol. Interact. 244 (2016) 140–148, https://doi.org/10.1016/j.cbi.2015.12.001.

[19] S. Mapoung, S. Suzuki, S. Fuji, A. Naiki-Ito, H. Kato, S. Yodkeeree, C. Ovatlarnporn, S. Takahashi, P. Limtrakul, Cyclohexanone curcumin analogs inhibit the progression ofcastration-resistantprostate cancer in vitro and in vivo, Cancer Sci. 110 (2019) 596–607, https://doi.org/10.1111/cas.13897.

[20] X. Wei, Z.Y. Du, X.X. Cui, et al., Effects of cyclohexanone analogues of curcumin on growth, apoptosis and NF-kappaB activity in PC-3 human prostate cancer cells, Oncol. Lett. 4 (2012) 279–284.

[21] R. Boudissa, A. Benmohammed, N. Chafai, A. Boudechicha, N. Rekiba, H. Lagraa, M. Achour, O. Khoumeri, A. Djafri, T. Terme, P. Vanelle, Synthesis, characterization, DFT, antibacterial, ADME-T properties, and molecular docking of new N-functionalized thiazolidinones, J.Mol.Struct. 1307 (2024) 138004, https://doi.org/10.1016/j.molstruc.2024.138004.

[22] S. Sathiyamoorthi, P. Srinivasan, Mater. Res. Innovat. 23 (6) (2019) 354–358, https://doi.org/10.1080/14328917.2018.1481600.

[23] S. Sathiamurthi, P. Srinivasan, J. Chem. Pharmaceut. Sci. 9 (2) (2016) 1017–1020.

[24] C. Dong, PowderX: windows-95-based program for powder X-ray diffraction data processing, J. Appl. Crystallogr. 32 (4) (1999) 838, https://doi.org/10.1107/S0021889899003039.

[25] C.F. Macrae, I. Sovago, S.J. Cottrell, P.T.A. Galek, P. McCabe, E. Pidcock, et al., Mercury 4.0: from visualization to analysis, design and prediction, J. Appl. Crystallogr. 53 (1) (2020) 226–235, https://doi.org/10.1107/S1600576719014092.

[26] Ma SY, Zheng Zb Fau - Sun Y-F, Sun Yf Fau - Wang Z-Y, Wang ZY. (2E,6E)-2,6-Difurfurylidenecyclo-hexa-none. (1600-5368 (Print)).

[27] G.H. Mahdavinia, M. Mirzazadeh, V. Amani, B. Notash, Acta Crystallogr., Sect. E: Struct. Rep. Online 68 (Pt 3) (2012) 778, https://doi.org/10.1107/S1600536812006629.

[28] G. Thirunarayanan, M. Gopalakrishnan, G. Vanangamudi, IR and NMR spectral studies of 4-bromo1-naphthyl chalcones-assessment of substituent effects, Spectrochim. Acta, Part A 67 (2007) 1106–1112.

[29] B.Z. Jovanovic′, M. Mišic′-Vukovic′, A.D. Marinkovic′, J. Csanadi, 13C NMR spectra of pyridine chalcone analogs, J. Mol. Struct. 482 (483) (1999) 371–374.

[30] G. Thirunarayanan, G. Vanangamudi, Synthesis of some 4-bromo-1-naphthyl chalcones using silica-sulfuric acid reagent under solvent free conditions, Arkıvoc xii (2006) 58–64.

[31] D. Hwang, J. Hyun, G. Jo, D. Koh, Y. Lima, Synthesis and complete assignment of NMR data of 20 chalcones, Magn. Reson. Chem. 49 (2011) 41–45.

[32] G. Vanangamudi, K. Ranganathan, G. Thirunarayanan, Synthesis, spectral and biological activities of some substituted styryl 2-phenothiazinyl ketones, World J. Chem. 7 (1) (2012) 22–33, https://doi.org/10.5829/idosi.wjc.2012.7.1.6328.

[33] R. Ravichandran, M. Rajendran, D. Devapiriam, Studies on chalcone derivatives antioxidant and stability constant, J Chem Bio Phy Sci Sec A 3 (4) (2013) 2446–2458.

[34] Srinath N. Synthesis, characterization and biological evaluation of some new chalcones [Cited 2014 May 2]; Available from: URL: http://shodhganga.inflibnet.ac.in/bitstream/10603/3446/10/10_chapter%201.pdf.

[35] V. Mala, K. Sathiyamoorthi, S.P. Sakthinathan, D. Kamalakkannan, R. Suresh, G. Vanangamudi, G. Thirunarayanan, Solvent-free synthesis, spectral correlations and antimicrobial activities of some 3,4-dimethoxychalcones, Q-Science Connect (2013), https://doi.org/10.5339/connect.2013.7.

[36] C. Van de Sande, J.W. Serum, M. Vandewalle, Studies in organic Mass spectrometry-XII: mass spectra of chalcones and flavanones. The isomerisation of 2'-hydroxy-chalcone and flavanone, Org. Mass Spectrom. 6 (1972) 1333–1345.

[37] D. Cremer, J.A. Pople, J.Amer.Chem.Soc. 97 (1975) 1354–1358.

[38] N.M. Abd El-Fadeal, M.S. Nafie, K. El-kherbetawy M, A. El-Mistekawy, H.M.F. Mohammad, A.M. Elbahaie, et al., Antitumor activity of nitazoxanide against colon cancers: molecular docking and experimental studies based on wnt/β-catenin signaling inhibition, Int. J. Mol. Sci. 22 (10) (2021) 5213, https://doi.org/10.3390/ijms22105213.

[39] S. Rajasekhar, S. Das, R. Karuppasamy, B. Musuvathi Motilal, K. Chanda, Identification of novel inhibitors for Prp protein of Mycobacterium tuberculosis by structure based drug design, and molecular dynamics simulationsJournal of Computational, Chemistry 43 (9) (2022) 619–630, https://doi.org/10.1002/jcc.26823.

[40] M. Hosseini, W. Chen, D. Xiao, C. Wang, SARS-CoV-2 drugs, Precision Clinical Medicine 4 (1) (2021) 1–16, https://doi.org/10.1093/pcmedi/pbab001.

[41] Lorraine M. Deck, Lucy A. Hunsaker, Thomas A. Vander Jagt, Lisa J. Whalen Robert E. Royerb, L. David, Vander Jagt"Activation of anti-oxidant Nrf2 signaling by enone analogues of curcumin", Eur. J. Med. Chem. V143 (2018) 854–865, https://doi.org/10.1016/j.ejmech.2017.11.048.

[42] Gehad Lotfy, Mohamed Said, El Sayed H. El Ashry, El Sayed H. El Tamany, YasmineM. Abdel Aziz, Saied M. Soliman, Abdullah Mohammed Al-Majid, Hazem Ghabbour, Assem BarakatSyntheses and X-ray crystal structures combined with conformational and Hirshfeld analyses of chalcones based on a cyclohexanone scaffold, Journal of molecular structure V1198 (2019) pp126873, https://doi.org/10.1016/j.molstruc.2019.126873.

[43] Nimisha Singh, Jyoti Pandey, Amit Yadav, Vinita Chaturvedi, Shalini Bhatnagar, N. Gaikwad Anil, SudhirKumar Sinha, Awaneet Kumar, P.K. Shukla, P. Rama, Tripathi A facile synthesis of α,α′-(*EE*)-bis(benzylidene)-cycloalkanones and their antitubercular evaluationsEuropean, J. Med. Chem. V44 (4) (2009) 1705–1709, https://doi.org/10.1016/j.ejmech.2008.09.026.

[44] U.P. da Silva, B.W. Ferreira, B.L. de Sousa, et al., Synthesis of bis(ylidene) cyclohexanones and their antifungal activity against selected plant pathogenic fungi, Mol Divers 27 (2023) 281–297. https://doi.org/10.1007/s11030-022-10431-7.

[45] M. Frisch, G.W. Trucks, H.B. Schlegel, G.E. Scuseria, M.A. Robb, J.R. Cheeseman, et al.. Gaussian 09, revision D. 01, Gaussian, Inc, Wallingford CT, 2009.

[46] J.C. Tai, N.L. Allinger, A theory for the quantitative calculation of the amplitudes of cotton effect curves of ketones, J. Am. Chem. Soc. 88 (10) (1966) 2179–2187, https://doi.org/10.1021/ja00962a020.

[47] A.P. Scott, L. Radom, Harmonic vibrational frequencies: an evaluation of Hartree−Fock, Møller−Plesset, Quadratic Configuration Interaction, Density Functional Theory, and Semiempirical Scale Factors, J. Phys. Chem. 100 (41) (1996) 16502–16513, https://doi.org/10.1021/jp960976r.

[48] G Varsányi, L Láng, Assignments for Vibrational Spectra of Seven Hundred Benzene Derivatives, 1, Wiley, 1974.

[49] Sajan D., Binoy J., Pradeep B., Venkata Krishna K., Kartha V.B., Hubert Joe I., Jayakumar V.S., (1386-1425 (Print)).

[50] M.C. Ruiz Delgado, V. Hernández, J. Casado, J.T. López Navarrete, J.M. Raimundo, P. Blanchard, et al., Vibrational study of push–pull chromophores for second-order non-linear optics derived from rigidified thiophene π-conjugating spacers, J. Mol. Str. 651-653 (2003) 151–158. https://doi.org/10.1016/S0022-2860(02)00644-0.

[51] K.R. Jennings, Spectrometric identification of organic compounds (Fifth Edition) R. M. SILVERSTEIN, G. C. BASSLER AND T. C. MORRILL. Wiley, New York, 1991. No. of pages: 430. ISBN 0471 634042, Org. Mass Spectrom. 26 (9) (1991) 813. https://doi.org/10.1002/oms.1210260923.

[52] J. Binoy, J.P. Abraham, I.H. Joe, V. Jayakumar, G. Pettit, O.F. Nielsen, NIR-FT Raman and FT-IR spectral studies and ab initio calculations of the anti-cancer drug combretastatin-A4, J. Raman Spectrosc. 35 (11) (2004) 939–946. https://doi.org/10.1002/jrs.1236.

[53] D. Sajan, J. Binoy, I. Hubert Joe, V. Jayakumar, J. Zaleski, NIR-FT Raman, FT-IR and surface-enhanced Raman scattering spectra of organic nonlinear optic material: p-hydroxy acetophenone, J. Raman Spectrosc. 36 (3) (2005) 221–236. https://doi.org/10.1002/jrs.1424.

[54] S. Sevvanthi, S. Muthu, M. Raja, Molecular docking, vibrational spectroscopy studies of (RS)-2-(tert-butylamino)-1-(3-chlorophenyl) propan-1-one: a potential adrenaline uptake inhibitor.J, Mol. Struct. 1173 (2018) 251–260. https://doi.org/10.1016/j.molstruc.2018.07.001.

[55] E. Cances, B. Mennucci, J. Tomasi, A new integral equation formalism for the polarizable continuum model: Theoretical background and applications to isotropic and anisotropic dielectrics, J. Chem. Phys. 107 (8) (1997) 3032–3041. https://doi.org/10.1063/1.474659.

[56] B. Mennucci, J. Tomasi, Continuum solvation models: A new approach to the problem of solute's charge distribution and cavity boundaries, J. Chem. Phys. 106 (12) (1997) 5151–5158. https://doi.org/10.1063/1.473558.

[57] R.A. Costa, P.O. Pitt, M.L.B. Pinheiro, K.M.T. Oliveira, K.S. Salomé, A. Barison, Spectroscopic investigation, vibrational assignments, HOMO-LUMO, NBO, MEP analysis and molecular docking studies of oxoaporphine alkaloid liriodenine, Spectrochim. Acta Mol. Biomol. Spectrosc. 174 (2017) 94–104. https://doi.org/10.1016/j.saa.2016.11.018.

[58] C.H. Choi, M. Kertesz, Conformational information from vibrational spectra of styrene, trans-stilbene, and cis-stilbene, J. Phys. Chem. A 101 (20) (1997) 3823–3831. https://doi.org/10.1021/jp970620v.

[59] S. Gunasekaran, S. Kumaresan, R. Arunbalaji, G. Anand, S. Srinivasan, Density functional therory study of vibrational spectra and assignment of fundamental modes of dacarbazine, J. Chem. Sci. 120 (3) (2008) 315–324. https://doi.org/10.1007/s12039-008-0054-8.

[60] R. Sathishkumar, C.J. Magesh, S. Tamilselvan, G. Lavanya, K. Venkatapathy, M. Vimalan, Synthesis, crystal structure, spectroscopic and docking studies of mononuclearmono(bis(2-(4-butylphenyl)imino)methyl)phenoxy)zinc(II)dichloride complexas a promising candidate for α-glucosidase inhibition, Chemical Data Collections 17-18 (2018) 187–195. https://doi.org/10.1016/j.cdc.2018.08.012.

[61] L. Padmaja, C. Ravikumar, D. Sajan, I. Hubert Joe, V.S. Jayakumar, G.R. Pettit, et al., Density functional study on the structural conformations and intramolecular charge transfer from the vibrational spectra of the anticancer drug combretastatin-A2, J. Raman Spectrosc. 40 (4) (2009) 419–428. https://doi.org/10.1002/jrs.2145.